JNCS Journal of Nepal Chemical Society January 2026, Vol. 46, No. 1, 41-50
ISSN: 2091-0304 (print)
DOI: https://doi.org/10.3126/jncs.v46i1.91121
RESEARCH ARTICLE

Incorporation of Carbon Quantum Dots into Cobalt Hydroxide for Supercapacitor Application

Govinda Thakur[1], Barsha Pandey[1], Netra Bahadur Khadka[1], Mohan Sharma[1], Kushal Chuwain Subedi[1], Babina Dahal[1], Bipeen Dahal*[1], Subhangi Subedi*[2]

[1]*Central Department of Chemistry, Tribhuvan University, Kirtipur, Kathmandu, Nepal*

[2]*Department of Chemistry, Tri-Chandra Multiple Campus, Tribhuvan University, Nepal*

[*]*Corresponding Email: bipeen.dahal@cdc.tu.edu.np/ subhangisubedi@gmail.com*

(Received: December 15, 2025 revised: January 15, 2026, accepted: January 25, 2026)

Abstract

The rapid depletion of non-renewable resources has stepped up the pursuit globally for effective and sustainable sources of energy. Herein, cobalt hydroxide [$Co(OH)_2$] incorporated with carbon quantum dots (CQDs) was synthesized via a single-step hydrothermal method and characterized for supercapacitor investigations. Structural characterization through X-ray diffraction (XRD) confirmed the crystallinity of cobalt hydroxide as well as the successful incorporation of CQDs without inhibiting its crystal structure. Scanning electron microscopy (SEM) confirmed the well-defined morphology of pure as well as composite material, whereas energy-dispersive X-ray (EDX) confirmed the anticipated elemental composition. Electrochemical behavior was analyzed by cyclic voltammetry (CV), galvanostatic charge-discharge (GCD), and Electrochemical impedance spectroscopy (EIS). The potential window of pure $Co(OH)_2$ was 0.6 V, with a specific capacitance of 800 F g^{-1} at 1 A g^{-1}, which declined to 350 F g^{-1} at 10 A g^{-1}. Notably, after the addition of CQD, the area of CV increased, and the optimized composite, $Co(OH)_2$/CQD (3), achieved a capacitance of 1300 F g^{-1} at 1 A g^{-1} and maintained 670 F g^{-1} at 10 A g^{-1}. The Ragone plot confirmed superior performance of the material with energy density up to 65 W h kg^{-1} and the power density of 4.044 kW kg^{-1}. The composite also retained 90.2% of the initial capacitance after 5000 repetitive charge-discharge cycles, showing excellent cycling stability. These findings highlight the potential of $Co(OH)_2$/CQD composites as a high-performance material for supercapacitors, offering a promising path to sustainable energy storage technology.

Keywords: Energy storage; Supercapacitor; Carbon quantum dot; Cobalt hydroxide; Hydrothermal

Introduction

One of the biggest obstacles to attaining sustainable growth is the scarcity of fossil fuels and the problem with proper energy harvesting and storage [1]. Fossil fuels not only produce harmful chemicals but also push the world from natural to natural calamities [2]. As a result, research into energy storage technologies and other energy sources is crucial. These alternative energy storage systems must meet a number of crucial requirements, such as high energy density, high power density, extended lifespan, environmental safety, and affordability [3].

The development of a renewable and environmentally friendly energy production and storage system is important in order to overcome the problems of energy crises and environmental pollution [4]. In this context, batteries, fuel cells, and electrochemical capacitors (ECs) are acknowledged as crucial electrochemical energy conversion and storage devices [5].

Supercapacitors (SCs) have garnered attention as excellent energy storage devices due to their numerous advantageous characteristics. These characteristics include high power density, rapid response times (with charging and discharging completed within

seconds), exceptional long-term cycle stability, and high reliability [6-7]. Based mostly on their charge storage mechanisms, SCs are often divided into three types: electric double-layer capacitors (EDLCs), pseudo-capacitors (PCs), and hybrid capacitors. Electrostatic interactions induce the buildup of electrolytic ions at the interface between the electrode and the electrolyte, creating a double layer, which is how EDLCs work [8]. In contrast, pseudo-capacitors mostly store energy by means of faradaic redox processes that take place at the active material's electrode surface as well as at the bulk [9]. On the other hand, hybrid capacitors consist of electrodes that store energy both by EDLC and pseudocapacitive mechanisms [10]. Supercapacitors perform in the middle of regular capacitors and batteries, as observed in the Ragone plot, which is used as a figure-of-merit for energy storage devices [11]. So, the recent research is targeted towards increasing the energy density of SCs by developing a suitable hybrid-composite electrode material [12].

Amorphous $Co(OH)_2$ is extensively used as a promising supercapacitor electrode material due to its exceptional electrochemical properties, like ultrahigh capacitance of 1094 F g^{-1}, 95% capacitive retention over 8000 cycles [13]. But it is also often combined with other electrode materials in order to increase the stability and eventually enhance the electrochemical performance beyond that of pristine. Jagtap et al. (2024) synthesized a hybrid electrode material, $Co(OH)_2$/rGO to gain an enhanced specific capacitance of 2688 F g^{-1} due to synergistic interaction between rGO and $Co(OH)_2$ [14]. In order to improve its suitability for supercapacitor applications, a single-step hydrothermal method was used to synthesize cobalt hydroxide incorporated with carbon quantum dots (CQD) because of the exceptional properties of CQD [15]. In comparison to pure $Co(OH)_2$, the study is concentrated on improving CQD loading to enhance electrical conductivity, specific capacitance, and rate capability.

Materials and methods

Chemicals

Commercially accessible chemicals and materials were used in this project. Sodium hydroxide (NaOH, 97%), anhydrous citric acid ($C_6H_8O_7$, 99.5%), and Cobaltous nitrate hexahydrate ($Co(NO_3)_2.6H_2O$, 97-101%) were bought from Thermo-Fisher Scientific India Pvt. Ltd. Ethanol (99.9%) was bought from Changshu Hongsheng Fine Chemical Co., Ltd. in Changshu, Jiangsu Province. All the chemicals were used from the Functional Nanomaterials Processing Lab, CDC, Kirtipur, as received.

Material Synthesis

Synthesis of CQD

For the synthesis of CQD, 2 g of citric acid was taken in a beaker and put on a hot plate with a magnetic stirrer at a temperature of 200 ℃. At that temperature, citric acid melted and turned pale yellow in color. The prepared ethanoic NaOH solution (1g / 100 mL) was added steadily to the boiling melt. The formed product was then centrifuged at 7000 rpm for 30 minutes, syringe filtered, followed by drying at 30 ℃ in a hot air oven overnight.

Synthesis of CQD incorporated Co $(OH)_2$ by one step hydrothermal method

For the synthesis of CQD incorporated Co $(OH)_2$, 1 mg of CQD was combined with solutions of sodium hydroxide and cobaltous nitrate hexahydrate in a beaker. After 10 minutes of stirring with a magnetic stirrer, the liquid was sonicated for a further 10 minutes. After that, the mixture was placed in a Teflon autoclave and a hydrothermal apparatus at 180 for 12 h. Similarly, the CQD concentration was adjusted to 2, 3, and 4 mg. Co $(OH)_2$,/CQD (1), Co $(OH)_2$,/CQD (2), Co $(OH)_2$,/CQD (3), and Co $(OH)_2$,/CQD (4) were the labels applied to the composites formed.

Preparation of the working electrode

Nickel foam (1 cm × 1 cm) was washed with 1 M HCl and deionized water in an ultrasonic bath. Then, it was carefully dried in an oven at

50 °C for 1 hour, and its weight was noted. A slurry of the electrode material was prepared by carefully weighing 4 mg (80 wt%) of the prepared active material, 0.4 mg (10 wt%) of binder (PVDF), and 0.4 mg (10 wt%) of conductive additive (active carbon) followed by grinding into fine slurry by dropwise addition of NMP solvent for at least 45 minutes using mortar and pestle. Then, the slurry was coated onto clean and dry nickel foam several times by quickly drying after each coating before applying the next one. After that, the electrode was wrapped in aluminum foil and subjected to pressing overnight. Next, the weight of the electrode was taken and dipped into 3 M KOH for at least 3 h before being subjected to electrochemical testing.

Structural and Morphological Characterization

A Rigaku Ultima Plus X-ray diffractometer (Rigaku Co., Japan) operating at 40 kV and 90 mA with Cu Kα radiation (λ = 0.154 nm) was used to obtain the XRD patterns of all the samples. A field emission scanning electron microscope (FE-SEM) equipped with an energy dispersive X-ray spectrometer (EDX), Hitachi S-7400, Japan, was used to examine the surface morphology, and a JEM-2100 plus transmission electron microscope was used to analyze the microstructure of CQD at Jeonbuk National University in the Republic of Korea.

Electrochemical Characterization

The electrochemical performance of the prepared electrode materials was examined using the three-electrode cell configuration, using a CHI 660E potentiostat with the working electrode made from the active material prepared, with a reference electrode being Hg/HgO, Pt wire as the counter electrode, and 3 M KOH as the electrolyte. Tests for cyclic voltammetry (CV), galvanostatic charge-discharge (GCD), and electrochemical impedance spectroscopy (EIS) were carried out to evaluate the electrochemical performance of the prepared electrode materials. Using the following equation, the Specific capacitance from the GCD data was determined:

$$Cs = \frac{I \times \Delta t}{\Delta V \times m} \quad \text{.....(1)}$$

where, I = discharge current (A), Δt= discharge time (s), ΔV= potential window (V), m = mass of the active material (g).

Similarly, Energy density (E, W h kg^{-1}) and power density (P, W kg^{-1}) of the electrode material were calculated using the discharge time (Δt, s) from the GCD curve.

$$E = \frac{1}{2}\frac{C_s \times \Delta V^2}{3.6} \quad \text{.....(2)}$$

$$P = \frac{E \times 3600}{\Delta t} \quad \text{.....(3)}$$

Also, the coulombic efficiency (CE) can be calculated as:

$$CE = \frac{t_{discharging}}{t_{charging}} \times 100\% \quad \text{.....(4)}$$

Results and Discussion

Physicochemical Characterization

Pure $Co(OH)_2$ shows distinct peaks **(Figure 1)** around 2θ = 19°, 31.1°, 36.8°, 55.5°, 59.2°, and 65.8° corresponding to the (001), (100), (101), (110), (003), and (200) planes, respectively in agreement with the JCPDS card No. **74-1057** for β -$Co(OH)_2$ [16]. Their characteristic peaks remain clearly visible in the composite, confirming that CQD incorporation does not alter the Co $(OH)_2$, crystal structure. A broad hump centered around 24.8° is the signature peak of carbon, indicating the incorporation of amorphous CQDs into the layered β- Co $(OH)_2$, [17]. The surface morphology of the synthesized samples was examined using SEM at 10,000× and 80,000× magnifications with an accelerating voltage of 10 kV and a 15 mm working distance. The micrographs reveal that Co $(OH)_2$ forms well-defined cubic particles. **Figure 2 (a)** shows a granular and crack-free surface with uniform substrate coverage and a porous network comprising nano-scale gaps and channels, favorable for electrolyte penetration in supercapacitor applications [18]. **Figure 2 (b)** displays nanoplates and nanoblocks ranging from 80-250 nm, with moderate polydispersity.

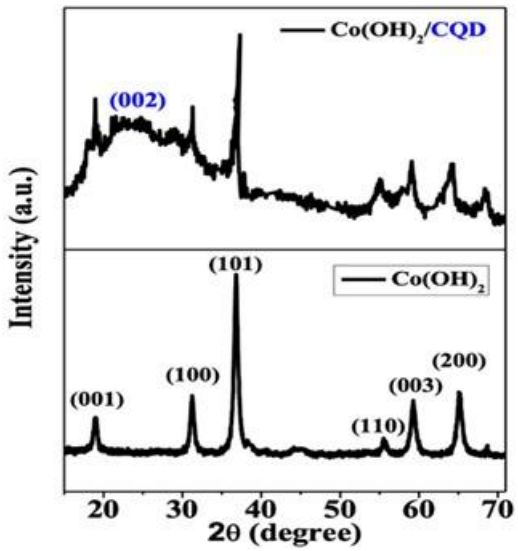

Figure 1: X-ray diffraction pattern of $Co(OH)_2$ and $Co(OH)_2$/CQD **(JCPDS card no. 74-1057)**

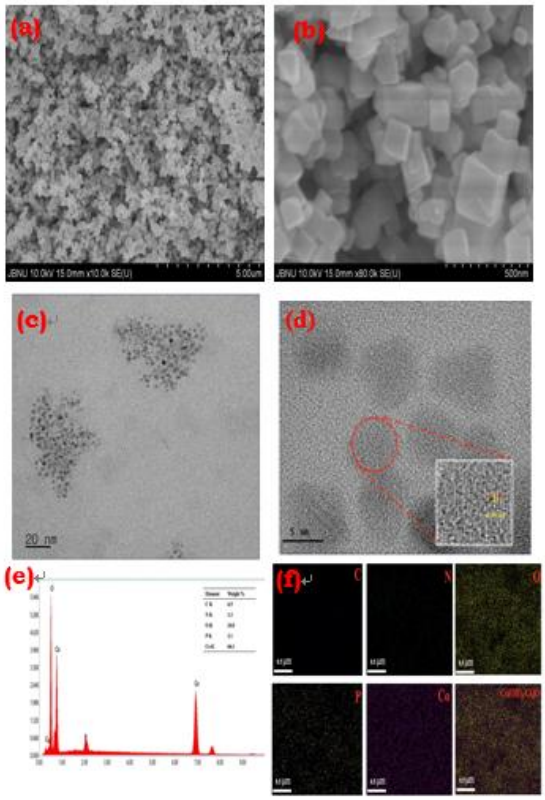

Figure 2: (a), (b) SEM images of $Co(OH)_2$/CQD (3), (c), (d) TEM images of CQD, and (e), (f) EDX and elemental mapping $Co(OH)_2$/CQD (3

Similarly, microstructure analysis was carried out using a JEM-2100 plus Transmission Electron Microscope at Jeonbuk National University, Republic of Korea. **Figure 2 (c)** shows the TEM image at a 20 nm scale, revealing uniformly dispersed CQDs appearing as small dark dots grouped into loose clusters with clear interparticle gaps [19]. The higher-magnification image in **Figure 2 (d)** exhibits well-defined lattice fringes with an interplanar spacing of 0.34 nm, corresponding to the (002) semi-crystalline carbon plane, consistent with the XRD findings [20].

The strong peaks at 6.9-7.0 keV and 0.78 keV in the EDX spectrum confirm the presence of cobalt, while the prominent oxygen peak at 0.52 keV corresponds to hydroxide groups, verifying the formation of cobalt hydroxide rather than metallic or oxide phases [21]. Minor foreign peaks appear with significantly lower intensities and do not affect the structural integrity of the composite [22]. The elemental composition of the sample is summarized in the inset of **Figure 2 (e)** with corresponding elemental mapping in **Figure 2 (f)**.

Electrochemical Characterization of the Prepared Samples

The shape of the resulting CV curve tells a story about the underlying charge storage process. For supercapacitor materials like $Co(OH)_2$, these redox peaks are often linked to reversible oxidation states of cobalt, while the introduction of CQDs can make the curves broader and more stable by enhancing electrical conductivity and offering more active sites [23]. In practical terms, the larger the enclosed area of the CV curve, the greater the stored charge, and therefore, the higher the capacitance [24].

The electrochemical performance for the $Co(OH)_2$ electrode was determined with the help of CV at scan rates of 5, 10, 20, 30, 40, and 50 mV s^{-1}, respectively, within a potential window of 0 to 0.6 V with Hg/HgO as a reference electrode, as illustrated in **Figure 3**. The CV curves display pronounced redox peaks in both the anodic and cathodic sweeps, confirming the pseudocapacitive nature of $Co(OH)_2$. At a lower scan rate, the well-defined redox peaks show that the electrolyte ions have enough time to permeate into the interior layers of the

electrode material, enabling almost full usage of the active sites whereas, the broadening of the curves at higher scan rate suggests that, while surface-controlled processes dominate at these speeds, deeper ion penetration is limited by diffusion kinetics [25]. CV was recorded for $Co(OH)_2$ with different amounts of CQD at a fixed scan rate (40 mV s^{-1}), which displayed quasi-rectangular but display broad redox features, consistent with a dominant pseudocapacitive process coupled with some electric-double-layer (EDL) contribution from the CQDs [26]. The presence of CQDs smooths and broadens the redox humps, reflecting faster electron transport and more accessible electroactive interfaces [27].

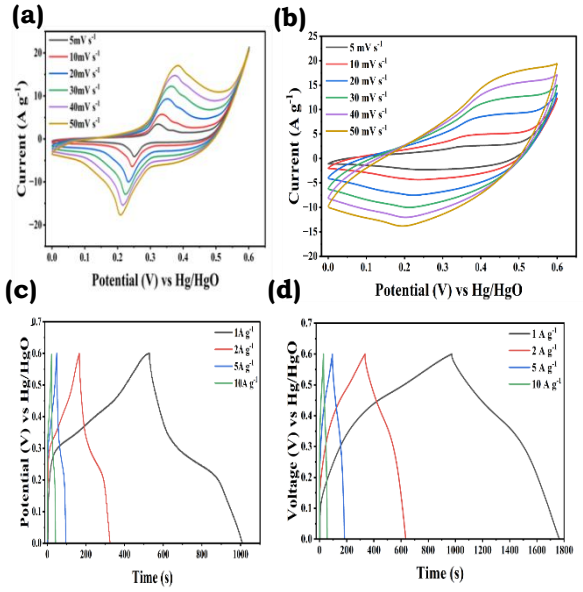

Figure 3: (a), (b) CV and (c), (d) GCD for $Co(OH)_2$ and $Co(OH)_2$/CQD (3)

After the incorporation of CQD, the anodic and cathodic currents, and consequently the enclosed CV area, increase significantly from 1 mg to 2 mg and reach a maximum at 3 mg, indicating the highest charge-storage capability [28]. Although the 4 mg sample maintains a high area, it shows a slight decline compared to 3 mg, suggesting that excessive loading surpasses the optimal threshold. Increasing CQD content improves the symmetry of CV loops and reduces the potential separation between redox peaks, reflecting lower polarization and faster charge-transfer kinetics due to CQDs acting as conductive bridges that enhance ion/electron transport [29]. Moderate CQD incorporation increases conductive pathways, improves wettability, and contributes additional EDL capacitance, while excessive amounts partially mask active $Co(OH)_2$ sites and hinder ion penetration, slightly reducing effective utilization [30]. Accordingly, for curves recorded at the same scan rate, the integrated CV area follows the order: 3 mg > 4 mg ≳ 2 mg > 1 mg. The quasi-rectangular CV shape with minor redox features confirms pseudocapacitive behavior driven by Co^{2+}/Co^{3+} transitions, and the proportional current increase with scan rate indicates good rate capability, fast kinetics, low internal resistance, and excellent electrochemical reversibility [31].

GCD involves charging the electrode with a constant current, then discharging it with the same current while monitoring the voltage over time. The resulting curve helps evaluate how well the material stores and releases charge, its stability, and overall performance.

The GCD curves of cobalt hydroxide at 1-10 A g^{-1} display non-linear, quasi-triangular profiles typical of pseudocapacitive materials, with noticeable asymmetry reflecting reversible Co^{2+}/Co^{3+} redox reactions [32]. At 1 A g^{-1}, the discharge time exceeds 1000 s, delivering the highest specific capacitance of 800 F g^{-1} due to efficient ion diffusion and full utilization of active sites. As the current density increases to 2, 5, and 10 A g^{-1}, the discharge duration shortens, and the capacitance correspondingly decreases to 530, 400, and 350 F g^{-1}, respectively, consistent with kinetic limitations and partial engagement of electroactive sites at faster rates. Nevertheless, cobalt hydroxide maintains relatively high capacitance even at 10 A g^{-1}, indicating strong rate capability.

For the $Co(OH)_2$-CQD (3) composite, the GCD curves across the same current range also exhibit non-linear profiles with mild charge-discharge asymmetry, confirming

pseudocapacitive behavior enhanced by the conductive CQDs [33]. The composite achieves its longest discharge time and highest capacitance of 1300 F g^{-1} at 1 A g^{-1}, reflecting superior ion accessibility and reduced internal resistance due to CQD incorporation. Capacitance decreases to 1000, 750, and 670 F g^{-1} at 2, 5, and 10 A g^{-1}, respectively, owing to kinetic constraints at higher rates. Despite this drop, the electrode retains over half of its rate capacitance even at tenfold higher current, demonstrating excellent rate performance enabled by improved electron transport and rapid redox kinetics within the composite [34].

Figure 4 (a) illustrates the current density-dependent capacitance of the $Co(OH)_2$/CQD composite, which also shows a decline with increasing current density. The composite achieves a maximum of 1300 F g^{-1} at 1 A g^{-1}, supported by improved conductivity and enhanced ion access provided by the CQDs. Capacitance decreases to 1000, 750, and 670 F g^{-1} at 2, 5, and 10 A g^{-1} due to ion-transport constraints at higher charge-discharge rates, where deeper active sites cannot fully participate. Nevertheless, the electrode maintains 51.5% of its initial capacitance at 10 A g^{-1}, demonstrating excellent rate performance enabled by the synergistic enhancement of electron transport and ion diffusion within the composite matrix [35]. Cyclic stability was seen with the continuous charge discharge, demonstrating the longevity and stability of the electrode materials. This test was conducted at a 1 A g^{-1} for 5000 cycles. The electrode material exhibits 90.2% retention after 5000 cycles as compared to the initial capacity, as shown in **Figure 4 (b)**.

Figure 4 (c) presents the Ragone plot of the $Co(OH)_2$/CQD (3) composite, illustrating the balance between energy density and power density to evaluate its suitability for high-performance energy-storage applications. The electrode delivers a maximum energy density of 65 W h kg^{-1} at 295.14 W kg^{-1}, demonstrating excellent low-rate storage capability.

As power density increases, the energy density gradually decreases, a typical trend in electrochemical systems, reaching 50 W h kg^{-1} at 594.32 W kg^{-1}, 37.50 W h kg^{-1} at 1452.97 W kg^{-1}, and 33.50 W h kg^{-1} at the highest tested power density of 4044.20 W kg^{-1}. This decline reflects the limited time available for complete energy release at high discharge rates. Despite this expected reduction, the composite retains comparatively high energy density across the power range, highlighting its strong potential for applications requiring both rapid charge-discharge capability and substantial energy storage [36].

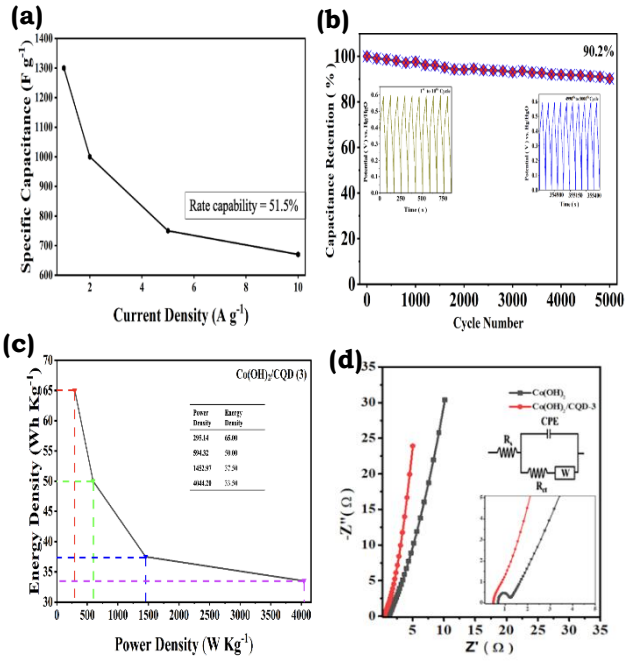

Figure 4: (a) Rate Capability, (b) Cyclic Stability, (c) Ragone plot, and (d) Nyquist plot for $Co(OH)_2$/CQD (3)

The coulombic efficiency of $Co(OH)_2$/CQD (3) composite was calculated to be 78.4% at 1 A g^{-1}, but increased to 83.2%, 85.5%, and 92.8% while current density increased to 2 A g^{-1}, 5 A g^{-1}, and 10 A g^{-1}, respectively. Therefore, it shows a good stability and reversibility of the material.

EIS assesses electrochemical systems by measuring impedance over a range of frequencies [37]. The Nyquist plots for pure $Co(OH)_2$ and the $Co(OH)_2$/CQD (3) as displayed in **Figure 4 (d)** composite reveal clear

distinctions in their electrochemical behavior. The equivalent circuit comprises solution resistance (R_s), charge-transfer resistance (R_{ct}), Warburg impedance (R_w), and a constant phase element (CPE), each representing key processes such as electrolyte resistance, interfacial charge transfer, ion diffusion, and non-ideal double-layer behavior.

In the high-frequency region, the composite shows a slightly lower R_s, indicating improved electrolyte-electrode interaction due to CQD incorporation [38]. The mid-frequency semicircle, associated with R_{ct}, is significantly smaller for the composite, confirming its faster and more efficient charge transfer [39]. At low frequencies, the steeper, more vertical slope of the composite reflects enhanced ion diffusion relative to pure $Co(OH)_2$ [40]. Overall, the incorporation of CQDs markedly enhances the electrochemical kinetics of $Co(OH)_2$, attributed to their excellent conductivity and electron mobility, resulting in a superior electrode material for high-performance energy-storage applications [41]. The R_s and R_{ct} values are evaluated using z-view and presented in the **Table 1.**

Table 1: R_s and R_{ct} values for the different electrodes

Electrodes	R_s (Ω)	R_{ct} (Ω)
$Co(OH)_2$	0.52	0.48
$Co(OH)_2$/CQD (3)	0.50	0.05

Conclusions

$Co(OH)_2$/CQD composites, synthesized by a one-step hydrothermal method, were characterized for their structural and electrochemical performance. With the introduction of amorphous carbon, the porosity and the conductivity of the compound increased while preserving the crystalline phase of $Co(OH)_2$. The $Co(OH)_2$/CQD (3) composite exhibited good rate capability with a specific capacitance of 1300 F g^{-1} at 1 A g^{-1} and retained 670 F g^{-1} even at 10 A g^{-1}. The Ragone plot revealed that the prepared material maintained 33.5 W h kg^{-1} of energy density with a power density of 4044 W kg^{-1} and delivered 65 W h kg^{-1} at 295 W kg^{-1}. Furthermore, the composite exhibited cycling stability with 90.2% retention after 5000 cycles with a high coulombic efficiency of 92.8% at 10 A g^{-1}. These results confirm that CQDs greatly improved the redox stability, conductivity, and ion transport, leading to superior charge-storage behavior. It can be concluded that the $Co(OH)_2$/CQD(3) composite showed an excellent prospect as a next-generation electrode material, which possessed excellent capacitance, long-lasting performance, and useful energy density.

Acknowledgements

This work has been carried out with the grants from OWSD-UNESCO, the International Development Research Centre, Canada, and the Nepal Academy of Science and Technology (NAST) young scientist grant. We are thankful to Jeonbuk National University, Republic of Korea for physicochemical and electrochemical characterizations

Author's contribution statement

G. Thakur: Laboratory work, methodology, software, data interpretation, writing original draft; **B. Pandey:** data curation, methodology, software, writing- review and editing, formal analysis; **N. B. Khadka:** formal analysis, software, visualization; **M. Sharma:** formal analysis, software, visualization; **K. C. Subedi:** formal analysis, software, visualization; **B. Dahal:** formal analysis, software, visualization; **B. Dahal**: conceptualization, data curation, supervision, project administration; **S. Subedi:** project administration, funding acquisition, validation, investigation, resources.

Conflict of interest

The authors do not have any conflict of interest pertinent to this work.

Data availability statement

The data that support the findings of this study

can be made available from the corresponding authors upon reasonable request.

References

[1] B. Dahal, T. Mukhiya, G.P. Ojha, A. Muthurasu, S. -H. Chae, T. Kim, D. Kang, H.Y. Kim, In-built fabrication of MOF assimilated B/N co-doped 3D porous carbon nanofiber network as a binder-free electrode for supercapacitors, *Electrochimica Acta,* 2019, *301*, 209–219. (DOI: 10.1016/j.electacta.2019.01.171)

[2] J. Zhang, Energy access challenge and the role of fossil fuels in meeting electricity demand: promoting renewable energy capacity for sustainable development, *Geoscience Frontiers,* 2024, *15* (5), 101873. (DOI: 10.1016/j.gsf.2024.101873)

[3] S. Ahmed, A. D'Angola, S. Ahmed, Energy storage systems: scope, technologies, characteristics, progress, challenges, and future suggestions—renewable energy community perspectives, *Energies,* 2025, *18* (11). (DOI: https://doi.org/10.3390/en18112679)

[4] K. K.Jaiswal, C. R. Chowdhury, D. Yadav, R. Verma, S. Dutta, K. S. Jaiswal, B. Sangmesh, K. S. K. Karuppasamy, Renewable and sustainable clean energy development and impact on social, economic, and environmental health, *Energy Nexus,* 2022, *7*, 100118. (DOI: https://doi.org/10.1016/j.nexus.2022.100118)

[5] T. Kousksou, P. Bruel, A. Jamil, T. El Rhafiki, Y. Zeraouli, Energy storage: applications and challenges, *Solar Energy Materials and Solar Cells,* 2014, *120*, 59–80. (DOI: https://doi.org/10.1016/j.solmat.2013.08.015)

[6] T. Kim, S. Subedi, B. Dahal, K. Chhetri, T. Mukhiya, A. Muthurasu, J. Gautam, P. C. Lohani, D. Acharya, I. Pathak, S. Chae, T. H. Ko, H.Y. Kim, Homogeneous elongation of N-doped CNTs over nano-fibrillated hollow-carbon-nanofiber: mass and charge balance in asymmetric supercapacitors is no longer problematic, *Advanced Science,* 2022, *9* (20), 2200650. (DOI: https://doi.org/10.1002/advs.202200650)

[7] Y. A. Kumar, G. R. Reddy, T. Ramachandran, D. K. Kulurumotlakatla, H. S. M. Abd-Rabboh, A. A. Abdel Hafez, S. S. Rao, S. W. Joo, Supercharging the future: MOF-2D MXenes supercapacitors for sustainable energy storage, *Journal of Energy Storage,* 2024, *80*, 110303. (DOI: https://doi.org/10.1016/j.est.2023.110303)

[8] M. Z. Ansari, S.A. Ansari, N. Parveen, M. W. Alam, S. -H. Kim, The role of high-entropy materials and D-band center adjustments in supercapacitor development, *Journal of Energy Storage,* 2025, *131*, 117535. (DOI: https://doi.org/10.1016/j.est.2025.117535)

[9] W. Pholauyphon, P. Charoen-amornkitt, T. Suzuki, S. Tsushima, Guidelines for supercapacitor electrochemical analysis: a comprehensive review of methodologies for finding charge storage mechanisms, *Journal of Energy Storage,* 2024, *98*, 112833. (DOI:https://doi.org/10.1016/j.est.2024.112833)

[10] J. Sung, C. Shin, Recent studies on supercapacitors with next-generation structures, *Micromachines,* 2020, *11* (12), 1125. (DOI: https://doi.org/10.3390/mi11121125)

[11] I. Beyers, A. Bensmann, R. Hanke-Rauschenbach, Ragone plots revisited: a review of methodology and application across energy storage technologies, *Journal of Energy Storage,* 2023, *73*, 109097. (DOI: https://doi.org/10.1016/j.est.2023.109097)

[12] S. Mandal, A. B. Mendhe, H. M. Rakhade, N. S. Barse, M. Roy, P. Rosaiah, T. Park, H. -S. Lee, A. C. Mendhe, D. Kim, Recent advancement and design in supercapacitor hybrid electrode materials: bridging the gap between energy and power density, *Chemical Engineering Journal Advances,* 2025, *21*, 100690.(DOI: https://doi.org/10.1016/j.ceja.2024.100690)

[13] H. B. Li, M. H. Yu, X. H. Lu, P. Liu, Y. Liang, J. Xiao, Y. X. Tong, G. W. Yang, Amorphous cobalt hydroxide with superior pseudocapacitive performance, *ACS Applied Materials and Interfaces,* 2014, *6* (2), 745–749.(DOI: https://doi.org/10.1021/am404769z)

[14] C. Jagtap, V. Kadam, B. Kamble, P. E. Lokhande, A. Pakdel, D. Kumar, R. Udayabhaskar, A. Vedpathak, N. B. Chaure, H. M. Pathan,

Synergistic growth of cobalt hydroxide on reduced graphene oxide/nickel foam for supercapacitor application, *Journal of Energy Storage,* 2024, *83*, 110666. (DOI: https://doi.org/10.1016/j.est.2024.110666)

[15] S. Subedi, A. K. Rella, L. G. Trung, V. Kumar, S. -W. Kang, Electrically switchable anisometric carbon quantum dots exhibiting linearly polarized photoluminescence: syntheses, anisotropic properties, and facile control of uniaxial orientation, *ACS Nano,* 2022, *16* (4), 6480–6492. (DOI: https://doi.org/10.1021/acsnano.2c00758)

[16] R. C p, J. K, A. P m, G. R. K, R. R b, Synthesis and characterization of alpha and beta cobalt hydroxide nanostructures for photocatalytic dye degradation and supercapacitor applications, *Next Materials,* 2024, *4*, 100199. (DOI: https://doi.org/10.1016/j.nxmate.2024.100199)

[17] S. Kumari, Sunaina, S. Devi, M. Jha, Design of new process for anchoring carbon quantum dots onto the cobalt oxyhydroxide surface for efficient oxygen generation, *Energy Fuels,* 2025, *39* (13), 6426–6437. (DOI: https://doi.org/10.1021/acs.energyfuels.4c05203)

[18] D. Ying, X. Zhou, Z. Liu, Applications of graphene in energy storage devices: from fundamental research to engineering practice, *Applied Energy,* 2026, *406*, 127243. (DOI: https://doi.org/10.1016/j.apenergy.2025.127243)

[19] Z. Ma, Y. Yu, S. Tao, X. Han, K. Zhang, B. Yang, Carbonized polymer dots: a class of highly functionalized nanoparticles with polymeric characteristics, *Polymer Science and Technology,* 2025, *1* (5), 436–457. (DOI: https://doi.org/10.1021/polymscitech.5c00036)

[20] D. K. Kar, P. V, S. Si, H. Panigrahi, S. Mishra, Carbon dots and their polymeric nanocomposites: insight into their synthesis, photoluminescence mechanisms, and recent trends in sensing applications, *ACS Omega,* 2024, *9* (10), 11050–11080. (DOI: https://doi.org/10.1021/acsomega.3c07612)

[21] E. Shanmugasundaram, K. Vellaisamy, V. Ganesan, V. Narayanan, N. Saleh, S. Thambusamy, Dual applications of cobalt-oxide-grafted carbon quantum dot nanocomposite for two electrode asymmetric supercapacitors and photocatalytic behavior, *ACS Omega,* 2024, *9*. (DOI: https://doi.org/10.1021/acsomega.3c09594)

[22] A. Longo, D. Mauri, C. J. Sahle, G. Tonsi, F. Bianconi, N. Ditaranto, S. Checchia, M. Scavini, M. Longhi, Shaping the empty carbon nanocubes: the role of nitrogen insight from X-ray Raman scattering spectroscopy at the N K-edge, *Carbon,* 2025, *240*, 120341. (DOI: https://doi.org/10.1016/j.carbon.2025.120341)

[23] J. Xiao, R. Momen, C. Liu, Application of carbon quantum dots in supercapacitors: a mini review, *Electrochemistry Communications,* 2021, *132*, 107143. (DOI: https://doi.org/10.1016/j.elecom.2021.107143)

[24] N. Arya, P. Avasthi, V. Balakrishnan, A light-fostered supercapacitor performance of multi-layered ReS_2 grown on conducting substrates, *Nanoscale Advances,* 2021, *3* (7), 2089–2102. (DOI: https://doi.org/10.1039/D0NA00901F)

[25] J. W.Gittins, K. Ge, C. J. Balhatchet, P. -L. Taberna, P. Simon, A. C. Forse, Understanding electrolyte ion size effects on the performance of conducting metal–organic framework supercapacitors, *Journal of the American Chemical Society,* 2024, *146* (18), 12473–12484. (DOI: https://doi.org/10.1021/jacs.4c00508)

[26] T. Kedara Shivasharma, R. Sahu, M.C. Rath, S. J. Keny, B. R. Sankapal, Exploring tin oxide-based materials: a critical review on synthesis, characterizations, and supercapacitive energy storage, *Chemical Engineering Journal.,* 2023, *477*, 147191. (DOI: 10.1016/j.cej.2023.147191)

[27] L. Li, C. Ding, W. Zha, High-entropy Ag, Pt-based catalyst toward exceptionally high-performance and stable electrochemical detection of nitrite, *Analytical Methods,* 2025, *17* (16), 3111–3117. (DOI: 10.1039/D5AY00257E)

[28] S. Sahoo, A. K. Satpati, P. K. Sahoo, P. D. Naik, Incorporation of carbon quantum dots for

improvement of supercapacitor performance of nickel sulfide, *ACS Omega,* 2018, *3* (12), 17936–17946. (DOI: 10.1021/acsomega.8b01238)

[29] F. F. Sead, Y. Jadeja, A. Kumar, R. M. M., M. Kundlas, S. Saini, K. K. Joshi, H. Noorizadeh, Carbon quantum dots for sustainable energy: enhancing electrocatalytic reactions through structural innovation, *Nanoscale Advances. 7* (13), 3961–3998. (DOI: https://doi.org/10.1039/d5na00205b)

[30] F. Tavakoli, A. A. Ensafi, B. Rezaei, Pine fruit activated carbon modified with $CuCo_2Se_4$ for the application in high-performance battery-type supercapacitor, *Scientific Reports,* 2025, *15*, 32211. (DOI: 10.1038/s41598-025-17938-7)

[31] S.A. Al-Shuayfani, S. T. Gunday, E. Cevik, M. A. Almessiere, A. Baykal, Fabrication of high-performance symmetric supercapacitor using hybrid cobalt spinel ferrite-decorated MoS_2 nanosheets, *Journal of Alloys and Compounds,* 2025, *1047*, 184960. (DOI: 10.1016/j.jallcom.2025.184960)

[32] E. Shanmugasundaram, K. Vellaisamy, V. Ganesan, V. Narayanan, N. Saleh, S. Thambusamy, Dual applications of cobalt-oxide-grafted carbon quantum dot nanocomposite for two electrode asymmetric supercapacitors and photocatalytic behavior, *ACS Omega,* 2024, *9* (12), 14101–14117. (DOI:10.1021/acsomega.3c09594)

[33] A. S. Raikwar, H. S. Panda, A review on nano-structured electrodes for high-performance supercapacitors: panoramic insights across dimensional spectra, *Discover Electronics,* 2025, *2* (1), 94. (DOI: https://doi.org/10.1007/s44291-025-00132-4)

[34] C. Wang, Z. Song, P. Shi, L. Lv, H. Wan, L. Tao, J. Zhang, H. Wang, H. Wang, High-rate transition metal-based cathode materials for battery-supercapacitor hybrid devices, *Nanoscale Advances,* 2021, *3* (18), 5222–5239. (DOI: https://doi.org/10.1039/D1NA00523E)

[35] P. Kumar, P. Sephra, M. Gupta, V. Jeoti, C. Tharini, G. M. Stojanović, Flexible and sustainable energy storage: recent progress and prospects in wearable supercapacitors, *Journal of Energy Storage,* 2026, *141*, 119173. (DOI: https://doi.org/10.1016/j.est.2025.119173)

[36] I. Pathak, D. Acharya, K. Chhetri, P. Chandra Lohani, S. Subedi, A. Muthurasu, T. Kim, T. H. Ko, B. Dahal, H. Y. Kim, $Ti_3C_2T_x$ MXene embedded metal–organic framework-based porous electrospun carbon nanofibers as a freestanding electrode for supercapacitors, *Journal of Materials Chemistry A,* 2023, *11* (10), 5001–5014. (DOI: https://doi.org/10.1039/D2TA09726E)

[37] H. S. Magar, R. Y. A. Hassan, A. Mulchandani, Electrochemical impedance spectroscopy (EIS): principles, construction, and biosensing applications, *Sensors,* 2021, *21* (19), 6578. (DOI: https://doi.org/10.3390/s21196578)

[38] M. S. Alva, R. A. Nazareth, Y. N. Sudhakar, N. Desai, Carbon quantum dot incorporated Xanthan gum based gel polymer electrolytes for high performance supercapacitors, *Scientific Reports,* 2025, *15*, 18227. (DOI: https://doi.org/10.1038/s41598-025-02341-z)

[39] I. Khan, D. Arif, A. U. Shah, K. Safeen, B. Ali, Gh. Eid, W. M. Girma, M. S. Khan, A. Y. Abid, A. Safeen, Superior electrochemical performance of $CuS/FeSe_2$ for advanced asymmetric supercapacitor applications, *Electrochemistry Communications,* 2025, *175*, 107915. (DOI: 10.1016/j.elecom.2025.107915)

[40] H. Jiang, J. Cheng, J. He, C. Pu, X. Huang, Y. Chen, X. Lu, Y. Lu, D. Zhang, Z. Wang, Y. Leng, P. K. Chu, Y. Luo, Cobalt–Nickel layered double hydroxides on electrospun MXene for superior asymmetric supercapacitor electrodes, *ACS Omega,* 2023, *8* (51), 49017–49026. (DOI: https://doi.org/10.1021/acsomega.3c06674)

[41] V. Osuna, C. Leyva-Porras, R. B. Dominguez, O. I. Torres-Soto, A. Vega-Rios, E. A. Zaragoza-Contreras, C. I. Piñón-Balderrama, Carbon quantum dot–supported nickel nanoparticles as a synergistic interface for electrochemical creatinine sensing, *Chemosensors,* 2025, *13* (12), 416. (DOI: 10.3390/chemosensors13120416)